Structures, Stabilities, and Electronic Properties of Endo- and Exohedral Complexes of T10−Polyhedral Oligomeric Silsesquioxane Cages

ARTICLE *in* THE JOURNAL OF PHYSICAL CHEMISTRY C · APRIL 2007

Impact Factor: 4.77 · DOI: 10.1021/jp068202q

3 AUTHORS, INCLUDING:

Charles U Pittman
Mississippi State University
582 PUBLICATIONS **14,784** CITATIONS
SEE PROFILE

Svein Saebo
Mississippi State University
94 PUBLICATIONS **2,746** CITATIONS
SEE PROFILE

Structures, Stabilities, and Electronic Properties of Endo- and Exohedral Complexes of T_{10}−Polyhedral Oligomeric Silsesquioxane Cages

Delwar Hossain,[†] Charles U. Pittman, Jr., and Svein Saebo*

Department of Chemistry, Mississippi State University, Mississippi State, Mississippi 39762

Frank Hagelberg

Computational Center for Molecular Structure and Interactions, Department of Physics, Atmospheric Sciences, and Geosciences, Jackson State University, Jackson, Mississippi 39217

Received: November 29, 2006; In Final Form: February 19, 2007

The geometries of endohedral and exohedral complexes of the polyhedral oligomeric silsesquioxane (POSS) cage molecule $(HSiO_{3/2})_{10}$ with the atomic or ionic species Li^0, Li^+, Li^-, Na^0, Na^+, Na^-, K^0, K^+, K^-, F^-, Cl^-, Br^-, He, Ne, and Ar have been optimized at the B3LYP/6-311G(d,p) level of theory. Single point MP2 calculations were carried out at the DFT-optimized geometries. The properties of these complexes depend on the nature of the species encapsulated in, or attached to, the $(HSiO_{3/2})_{10}$ cage. Encapsulation of noble gas atoms (He, Ne, and Ar) has almost no effect on the cage geometry. Encapsulation of alkali metal cations, in contrast, exhibits attractive interactions with cage oxygen atoms and leads to cage shrinkage. Encapsulation of halide ions results in cage expansion. Endohedral Li^+, Li^-, Na^+, F^-, Cl^-, and Br^- complexes are energetically favored relative to the separated species. The fluoride ion is predicted to migrate into the $(HSiO_{3/2})_{10}$ cage with little or no energy barrier with the cage remaining intact. The very low ionization potentials of endohedral Li^0, Na^0, and K^0 complexes suggest that enclosed alkali metals behave like "superalkalis". Overall, many of the endohedral complexes with small guest species appear to be viable synthetic targets.

I. Introduction

Polyhedral oligomeric silsesquioxane (POSS) systems represent an important class of nanocompounds with cage-shaped structures. Therefore POSS systems have been widely investigated in hybrid inorganic/organic polymers and nanocomposites. The building block of the H-silesquioxanes is the trifunctional monomer unit $(HSiO_{3/2})$ and the letter T is used to describe this unit.[1−4] If a POSS molecule is comprised of n $(HSiO_{3/2})$ units, the notation T_n−POSS is used to describe this system. For example, the T_{10} cage contains 10 silicon and 15 oxygen atoms with each cage silicon attached to one hydrogen outside the cage. According to Agaskar and Klemperer,[5] POSS systems can also be described by a topological descriptor $\{r^n s^m ...\}$, which indicates the number of r- and s-membered rings (faces) that comprise the polyhedron T_n. For example, the T_{10}−POSS cage D_{5h} isomer has the toplogical descriptor $\{6^0 5^2 4^5\}$ (no six-membered, two five-membered, and five four-membered rings). In its stable D_{5h} form, the T_{10}−POSS system consists of two double five-membered rings (D5R) with stoichiometry Si_5O_5 and linear Si−O−Si sides (see Figure 1). These two double five-membered rings are connected with five bridging oxygen atoms or with five fused double four-membered rings (D4R) each with stoichiometry Si_4O_4.

POSS derivatives incorporated into organic polymers, dendrimers, and zeolites have a variety of applications in materials science and catalysis.[4,6−15] POSS compounds have also emerged as viable fillers in high-performance nanocomposites.[1] POSS polymer nanocomposites are substantially harder than the unfilled polymers.[3] Incorporation of POSS cages into the polymeric materials enhances certain properties such as glass transition temperatures, decomposition temperatures, and mechanical strength.[16−19] In POSS PEO-based polymer electrolytes, POSS acts as an inhibitor to polyethylene oxide (PEO) crystallization.[2] POSSs are being used for synthesis of polymer-derived ceramics because of their nanosized structure and ceramic-like composition.[20] Metal-containing siloxanes and oligometallasilosesquioxanes have been reported as catalysts in olefin processing. For example, metathesis and epoxidation of alkenes have been accomplished with POSS derivatives.[21−25] POSS species have also been used to support Ziegler−Natta catalysts.[26] The cage structures of POSSs make them useful substances for separating gas mixtures with silicon-based capillary membranes,[27,28] and they can also serve as carriers and potential drug delivery agents.[29] Xiang et al.[30] studied the structural and electronic properties of different H-silsesquioxanes and Cheng et al.[31] reported the linear and nonlinear optical properties of H-silsesquioxanes.

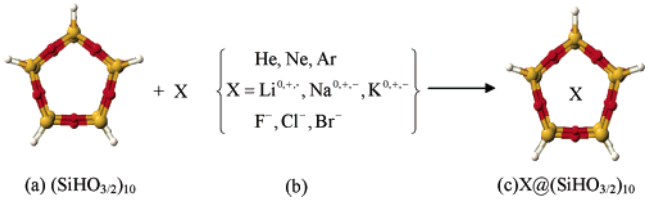

Figure 1. Schematic representation of the host cage $(SiHO_{3/2})_{10}$ with D5R units and the encapsulated species: (a) host cage with D_{5h} symmetry, (b) identity of X, and (c) endohedral species of $X@(SiHO_{3/2})_{10}$.

Space-filling models of POSS cages indicate there is a void at the center of the cube, but it is questionable whether this

[†] Department of Chemistry, Jahangirnagar University, Savar Dhaka 1342, Bangladesh.

10.1021/jp068202q CCC: $37.00
Published on Web 04/11/2007

space could be filled with an atomic species. Pach and Stosser[32] suggested that γ-irradiation of octaalkyl(T_8)silsesquioxane or octatrialkylsiloxy(T_8)silsesquioxane leads to encapsulation of a hydrogen atom, and ESR spectroscopy confirmed that a hydrogen atom had migrated from a peripheral organic substituent into the cage.

The size of the POSS cage plays a decisive role in both the structural and catalytic behavior of these micro porous solids.[33] An interesting question is what might happen upon encapsulation of atoms, ions, or molecules inside the cage. Previous experimental and theoretical studies have been largely limited to T_8−POSS systems. Bassindale et al.[34] recently synthesized and thoroughly characterized the endohedral complex of a fluoride ion and the T_8−POSS cage. Several theoretical studies of T_8−POSS complexes have been reported[33,35−37] including studies of Na^+, F^-, and OH^- endohedral complexes with hydroxy-substituted double four-membered ring (D4R) silsesquioxanes,[33] the insertion mechanism of N_2 and O_2 into T_n−POSS ($n = 8$, 10, 12),[35] and the binding strength of T_8−POSS cationic complexes. Recently,[36] we investigated the behavior and properties of both endohedral and exohedral Li^+, Na^+, K^+, F^-, Cl^-, Br^-, He, Ne, and Ar complexes of T_8−POSS. In contrast to T_8−POSS complexes, the interest in T_{10}−POSS complexes is relatively recent (see below).

In the discussion below the following questions will be addressed: Is the T_{10}−POSS cage stable when different cations and anions are incorporated into the cage? What kind of interactions occur between the encapsulated ion (or atom) and the T_{10}−POSS skeleton? Since very little is known about these systems, and because T_{10}−POSS has a larger cavity than its T_8 analogue, T_{10}−POSS complexes are ideal candidates for studies. In this paper we present results from theoretical studies of the stabilities and geometric, energetic, and electronic properties of both exohedral and endohedral complexes of T_{10}−POSS. Throughout this paper the endohedral complexes are denoted by X@T_{10}−POSS and exohedral by XT_{10}−POSS.

The parent cage, $(HSiO_{3/2})_{10}$, can, in principle, have several isomers. The most stable isomer has D_{5h} symmetry with $\{4^5 5^2\}$ topology and this is also the only isomer known experimentally.[5] The existence of two additional isomers of $(HSiO_{3/2})_{10}$ has been suggested by theoretical calculations. Both these structures have C_{2v} symmetry with $\{3^2 4^3 6^2\}$ and $\{3^4 4^1 7^2\}$ topology, respectively.[35,38] Calculations at the MP2 level predicted the D_{5h} form of T_{10}−POSS to be more stable than the two C_{2v} isomers by 18.0 and 42.7 kcal/mol, respectively.[35] Hence, in this work the D_{5h} structure was used as a starting point in all the calculations.

II. Computational Details

All geometries were optimized with density functional theory (DFT/B3LYP).[39,40] For the system studied herein, an explicitly correlated method like MP2 would have been desirable. However, full geometry optimization at the MP2 level was found too expensive for this study. Instead, single-point MP2 calculations at the DFT geometries were carried out for all systems. The 6-311G(d,p)[41] basis was employed for all calculations reported here and the unrestricted formalism was used for open shell species. Preliminary calculations on the T_{10}−POSS cage and selected endohedral complexes were carried out at both the Hartree−Fock and B3LYP levels with several smaller and larger basis sets. The results did not differ significantly from the B3LYP/6-311G(d,p) results. Therefore, only the B3LYP/6-311G(d,p) results and the results from the single-point MP2 calculations will be discussed here. For all optimized structures, harmonic vibrational frequencies were calculated at the same level mainly to verify that the optimized structure was a minimum on the molecular potential surface. In the cases where the optimized structure had imaginary frequencies, the structure was distorted and reoptimized until a structure with no imaginary frequencies was found. Gaussian-03[42] and PQS[43] ab initio programs were used to perform the calculations.

Three relative energies will be discussed: the inclusion energy for endohedral complexes, E_{inc}, the binding energy for exohedral complexes, E_{bind}, and the isomerization energy, E_{iso}. These are defined as

$$E_{inc} = E_{endo} - (E_{cage} + E_X) + \Delta E_{ZP} \quad (1)$$

$$E_{bind} = E_{exo} - (E_{cage} + E_X) + \Delta E_{ZP} \quad (2)$$

$$E_{iso} = E_{exo} - E_{endo} + \Delta E_{ZP} = E_{bind} - E_{inc} + \Delta E_{ZP} \quad (3)$$

respectively. E_X is the total energy of the guest species X, E_{cage} is the energy of the empty T_{10}−POSS cage, and E_{endo} and E_{exo} are the total energies of the endohedral and exohedral complexes, reaspectively. ΔE_{ZP} represents the difference in zero-point vibrational energies. Nuclear magnetic shielding tensors for selected systems were calculated with B3LYP/6-311G(d,p) and the GIAO method,[44−47] and electronic properties were evaluated with natural bond orbital analysis (NBO).[48]

The magnitude of the basis set superposition errors (BSSE) was estimated by the Boys−Bernardi counterpoise method.[49] The BSSE errors were significant (see Table 3), and a brief discussion about their significance is included below.

III. Results and Discussion

Geometries. The optimized geometrical parameters for the D_{5h} form of the parent T_{10}−POSS cage as well as all the endohedral complexes are summarized in Table 1, and the minimum energy structures for all endohedral and exohedral complexes are shown in Figures 2 and Figure 3, respectively.

Host Cage. The T_{10}−POSS cage in its stable D_{5h} form consists of two $(-SiH-O-)_5$ rings bridged by 5 oxygen atoms. The bridging oxygens are denoted O_b while the D5R oxygens are denoted by O throughout this text. Our calculated geometrical parameters (Table 1) are consistent with previous experimental[50] and theoretical[35,51] results. Typical Si−O bond lengths in the D5R and D4R frames are 1.64 Å. Previous theoretical studies[52−54] yielded Si−O distances of 1.62 to 1.64 Å. This agrees with the experimental X-ray diffraction values (Si−O = 1.62 Å).

Endohedral X@T_{10}−POSS Complexes with Alkali Metals. The endohedral complexes of the alkali metal ions Li^+, Na^+, and K^+ and the T_{10}−POSS cage as well as the corresponding neutral complexes were investigated. Negatively charged complexes with the same three alkali metals were also considered. These complexes could formally be considered as endohedral complexes of Li^-, Na^-, and K^- even though the alkali metals' negative oxidation states are unlikely. Among the endohedral X@$(HSiO_{3/2})_{10}$ complexes of alkali metals, the parent cage's D_{5h} symmetry was conserved only for X = Na^-, K^+, K, and K^- (see Figure 2). The D_{5h} structures of the endohedral complexes with Li, Li^+, Li^-, Na^+, and Na complexes were found to have between one and seven imaginary frequencies. When the symmetry constraints of these structures were removed, subsequent optimization of the structures resulted in geometries which were minima on the respective molecular potential surfaces. The distortions from the initial D_{5h} structures were quite significant for all three endohedral lithium complexes

TABLE 1: Molecular Point Groups, Selected Bond Lengths (Å), and Bond Angles (deg) of the $(HSiO_{3/2})_{10}$ Cage and Endohedral $X@(HSiO_{3/2})_{10}$ Complexes Calculated at the B3LYP/6-311G(d,p) Level

	sym	X−Si	X−O	X−O_b	Si−O	Si−O_b	Si−H	OSiO	SiO_bS	SiOSi	HSiO
cage	D_{5h}	3.155	2.980	3.121	1.637	1.642	1.462	110.0	152.0	155.9	109.6
Li^+	C_1	2.980	3.051	3.462	1.684	1.639	1.457	108	130.6	143.0	112.1
Li^0	C_1	2.522−3.220	3.220−3.239	3.220−3.239	1.663	1.636−1.655	1.463	105.9	150.4	125.5	111.4
Li^-	C_1	2.741	3.133	3.133	1.679	1.621	1.466	108.3	140.3	126.7	109.7
Na^+	C_1	3.223−3.198	2.411	3.376	1.667	1.667	1.458	108.9	136.6	153.6	113.0
Na^0	C_1	2.948−2.950	2.706	3.211−3.209	1.647	1.650	1.462	109.0	149.7	155.8	109.3
Na^-	D_{5h}	3.140	3.085	3.207	1.654	1.657	1.470	112.4	145.3	149.2	146.8
K^+	D_{5h}	3.201	2.875	3.224	1.649	1.649	1.456	106.8	148.8	164.8	112.5
K	D_{5h}	3.199	2.843	3.299	1.647	1.652	1.456	106.5	143.8	167..8	113.0
K^-	D_{5h}	3.194	2.824	3.341	1.645	1.656	1.456	106.1	140.9	170.1	113.3
F^-	C_s	3.027−3.162	3.004	3.008	1.636	1.470	1.472	112.2	150.6	147.8	106.9
Cl^-	D_{5h}	3.126	3.130	3.130	1.645	1.648	1.471	111.9	149.2	148.3	105.8
Br^-	D_{5h}	3.183	3.148	3.148	1.650	1.652	1.471	111.9	148.6	148.2	105.6
He	D_{5h}	3.157	2.982	2.982	1.638	1.642	1.462	109.2	152.3	155.9	109.7
Ne	D_{5h}	3.158	2.987	2.987	1.639	1.643	1.462	109.2	152.5	155.7	109.6
Ar	D_{5h}	3.168	3.031	3.031	1.645	1.647	1.462	109.7	153.7	154.9	109.3

while the geometry change differed only slightly from D_{5h} symmetry for the sodium complexes (see Figure 2).

Naturally, the bond distances and bond angles change after insertion of different atoms or ions into the T_{10} cage as shown in Table 1. The ten D5R frame oxygens (O) were closer to the cation than the five bridging oxygens (O_b), and the bridging oxygens have moved slightly outward compared to the empty cage. The calculated geometrical trends for the endohedral alkali metal complexes are complicated by the fact that the Li^+ complex exhibits large distortions from D_{5h} symmetry. The small Li^+ cation is a "hard" acid. This provides a strong driving force to distort the cage to allow the Li^+ ion to interact with some of the cage oxygens. The Si−H bond distance of 1.462 Å in the parent cage shortens for the Li^+, Na^+, and K^+ endohedral complexes to 1.457, 1.458, and 1.458 Å, respectively. Endohedral cations increase the Si−O bond lengths and the Si−O−Si angles while decreasing the O−Si−O angles.

Endohedral $X@T_{10}$−POSS Complexes with Halide Ions. The D_{5h} symmetry was conserved for both the endohedral Cl^- and Br^- complexes while the fluoride complex distorted to a system with C_s symmetry. The D5R framework oxygen to halide distances (X−O) have values of 3.004, 3.130, and 3.148 Å for X = F^-, Cl^-, and Br^-, respectively, versus 2.980 Å for the center of cage to O distance in the empty cage. Thus, the larger the anion size, the greater the cage expansion. After halide insertion the Si−O distance (originally 1.637 Å) becomes 1.636 (F^-), 1.645 (Cl^-), and 1.650 Å (Br^-). Pronounced changes occur in bond angles. The Si−O−Si angles increase while the O−Si−O angles decrease significantly upon intercalation of halides.

Endohedral $X@T_{10}$−POSS Complexes with Noble Gases. The D_{5h} symmetry of the parent cage was conserved for all endohedral noble gas complexes. The changes in the geometry of the POSS−T_{10} cage upon insertion of noble gases are remarkably small. The Si−O_b distance in the parent POSS−T_{10} cage is 1.637 Å while these distances expand to 1.638, 1.639, and 1.645 Å for the He, Ne, and Ar complexes, respectively. The minor structural changes indicate that negligible electron transfer occurs between the cage atoms and the encapsulated He, Ne, and Ar atoms. This is also confirmed by the calculated atomic charges (see below). The changes in bond angles were also very small as can be seen from Table 1. These results are not surprising since the noble gas atoms He, Ne, and Ar are all small and among the guest species investigated here only the Li^+ ion is smaller than Ar. The bond lengths in Table 1 suggest a small cage expansion for the endohedral Ar complex suggesting that larger noble gases (Kr or Xe) would probably not fit inside the cage.

Exohedral Clusters $X(HSi3/2)_{10}$. Table 2 summarizes selected geometric parameters for the exohedral $X(HSiO_{3/2})_{10}$ complexes of alkali metal cations, halides, and noble gases. The exohedral complexes are shown in Figure 3. When an exohedral complex is formed, the host cage's high D_{5h} symmetry is removed. The Si−X bond lengths for the exohedral complexes are 2.783, 3.169, and 3.567 Å for X = Li^+, Na^+, and K^+, respectively. These bond lengths are similar to those predicted in the corresponding endohedral systems. With the exception of these alkali metal ion complexes and the bromide complex the calculated distances between the cage and the exohedral atom were quite long. Since the computation method used neglects dispersion type interactions, the exohedral chloride and noble gas complexes may be artifacts of the method used in the present study.

Energetics. The inclusion, E_{inc}, binding, E_{bind}, and isomerization, E_{iso}, energies were defined in eqs 1−3 above and their values for both endohedral and exohedral complexes are shown in Table 3. A negative inclusion or binding energy means that the complex is more stable than the separated species, and a negative isomerization energy means that the exohedral complex is more stable than the corresponding endohedral one.

The relative energies were calculated both at the B3LYP-level and at the MP2-level with use of the B3LYP optimized geometries. Both are shown in Table 3 and the MP2 results will be used in the discussion below.

The BSSE for selected systems have also been included in Table 3. These are quite significant in some cases but they do not change any of the trends discussed below. For all the noble gas complexes, except the endohedral argon complex, the calculated inclusion and binding energies are small and of about the same magnitude as the BSSE. On the basis of our calculations we can therefore only conclude that the energies of these complexes are essentially the same as the energies of the corresponding separated species., and we can therefore not predict whether or not exohedral complexes with noble gases exist. The endohedral argon complex has significantly higher energy that the separated species.

The inclusion energies reveal that the endohedral Li^+, Li^-, Na^+, F^-, Cl^-, and Br^- complexes are more stable than their respective separated species, while all the remaining complexes are less stable. The endohedral F^- complex is exceptionally stable. The values of E_{inc} in Table 3 show that the endohedral

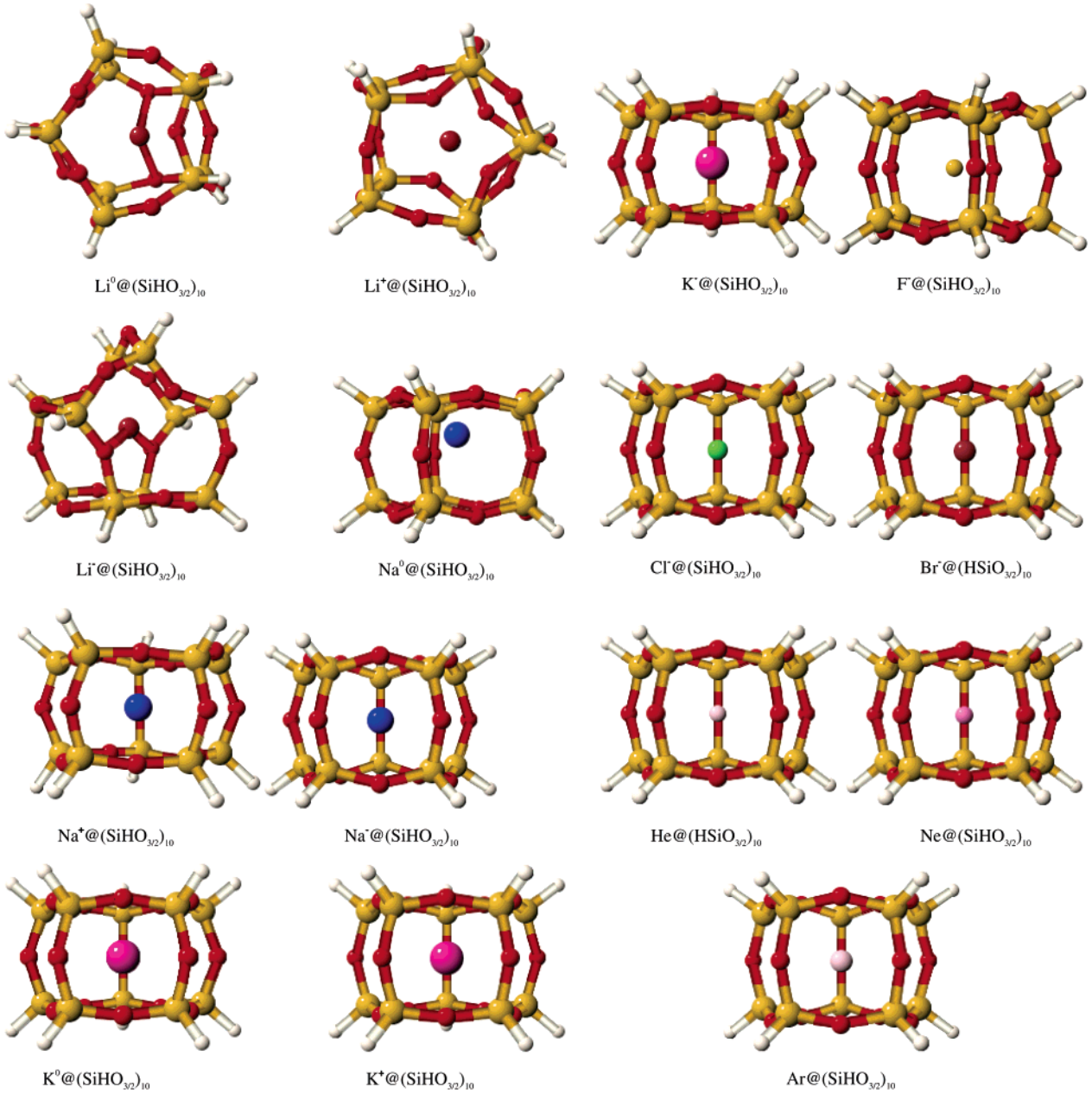

Figure 2. Optimized geometries of endohedral $X@(HSiO_{3/2})_{10}$ complexes of Li^0, Li^+, Li^-, Na^0, Na^+, Na^-, K^0, K^+, K^-, F^-, Cl^-, Br^-, He, Ne, and Ar, at the B3LYP/6-311G(d,p) level.

complexes become more stable as the size of X decreases within its periodic table group.

Among the intercalated species studied here, there are three sets of isoelectronic species: (He, Li^+), (F^-, Ne, Na^+), and (Cl^-, Ar, K^+). For the two sets containing anions, the endohedral complexes with anions are significantly more stable than their neutral and positively charged isoelectronic analogues in spite of the fact that the negative ions have the largest size within each set. The calculated atomic charges are −0.8 on halide ions, zero on noble gases, and +0.9 on encapsulated alkali ions for all endohedral complexes. Two effects contribute to the stability of endohedral complexes: a size effect and an electronic or electrostatic effect. Endohedral complexes of charged species appear to be more stable than neutral ones and, in general, complexes of anions are more stable than complexes of cations of comparable size. There is also a clear size effect as the stabilities of endohedral complexes decrease from one period to the next higher period. The stability order predicted for alkali cation $X@(HSiO_{3/2})_{10}$ complexes ($X = Li^+ > Na^+ > K^+$) in this work is related to that found by Sun et al.[55] from density functional calculations on alkali metal ion endohedral C_{32} cage complexes ($Li^+@C_{32}$, −53.1 kcal/mol; $Na^+@C_{32}$, −26.9 kcal/mol, $K^+@C_{32}$, 13.7 kcal/mol). The inclusion energies for the endohedral complexes may be compared with those of endohedral dodecahedrane complexes $X@C_{20}H_{20}$[56] and endohedral T_8−POSS[36] complexes. The endohedral complexes of Li^+ and Na^+ and T_{10}−POSS are considerably more stable (Li^+, −61.4 kcal/mol; Na^+, −28.5 kcal/mol) than the corresponding T_8−POSS analogues (Li^+, −18.5 kcal/mol; Na^+, 11.3 kcal/mol). This is not a surprise due to the larger cage size of the T_{10}−POSS systems. The endohedral T_{10}−POSS complexes are also more stable (lower inclusion energies) than the known dodecahedrane $C_{20}H_{20}$ complexes (Li^+, −12.7 kcal/mol; Na^+, 55.3 kcal/mol)[56] and the same trends were also found for the noble gas inclusion energies

Calculations on exohedral complexes with noble gases suggested that if any of these did in fact exist there are only weak interactions between the noble gas and the cage. As

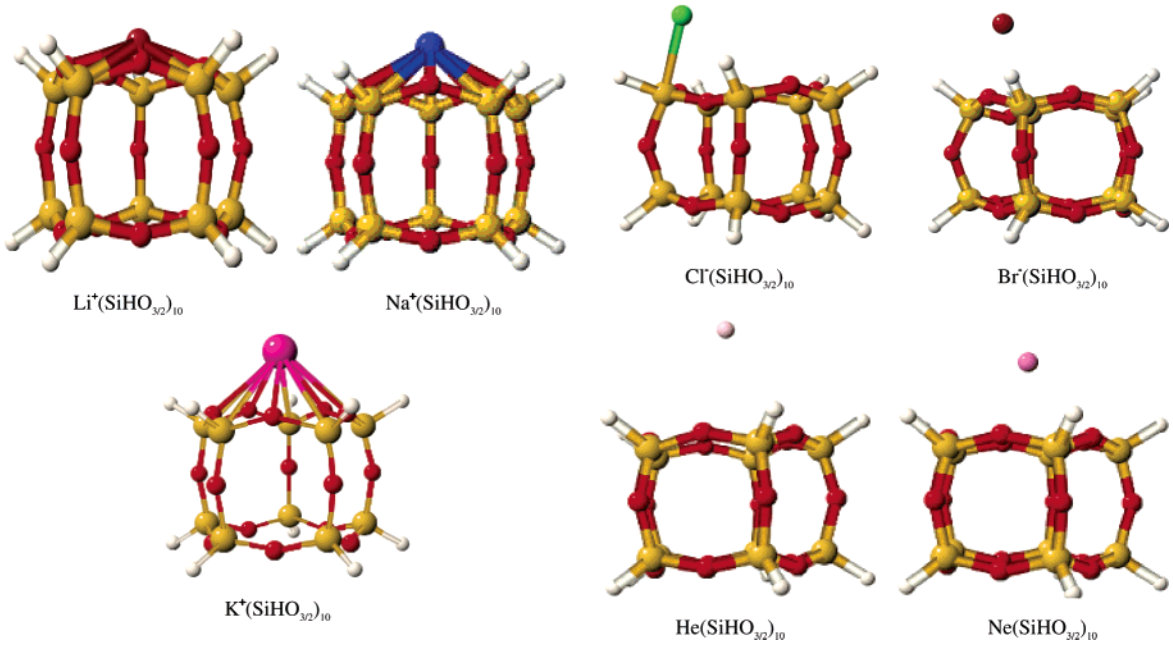

Figure 3. Optimized geometries of exohedral T_{10}−POSS complexes $X(HSiO_{3/2})_{10}$ of Li^+, Na^+, K^+, Cl^-, Br^-, He, and Ne calculated at the B3LYP/6-311G(d,p) level of theory.

TABLE 2: Molecular Point Groups, Selected Bond Lengths (Å), and Bond Angles of the $(HSiO_{3/2})_{10}$ Cage and Exohedral $X(HSiO_{3/2})_{10}$ Complexes Calculated at the B3LYP/6-311G(d,p) Level

	sym	X−Si[a]	X−O[a]	Si−O	Si−O_b	Si−H	OSiO	SiO_bS	SiOSi	HSiO
Li^+	C_1	2.783	2.001	1.636−1.688	1.621−1.662	1.457−1.458	107.2−112.1	157.3−175.7	150.0−157.7	110.0−112.2
Na^+	C_{5v}	3.169	2.479	1.634−1.664	1.617−1.658	1.458−1.459	110.7−111.2	160.5	148.7−154.9	112.2−109.9
K^+	C_{5v}	3.567	2.888	1.634−1.660	1.618−1.655	1.458−1.460	107.5−111.2	162.1	147.7−153.7	110.1−112.0
Cl^-	C_1	2.486	2.925	1.611−1.670	1.641−1.664	1.463−1.468	107.0−110.6	137.2−150.7	147.7−156.4	108.3−109.3
Br^-	C_1	3.452	3.297	1.629−1.641	1.631−1.683	1.464-1.468	105.5−110.0	137.4−150.4	148.3−156.0	108.5−108.4
He	C_1	4.590	4.047	1.637	1.642	1.462	109.1−109.4	152.3−152.5	155.3	109.5−109.6
Ne	C_{5v}	3.813	3.259	1.637	1.642	1.442	109.2	152.2	152.8−152.9	109.8

[a] The shortest X−Si and X−O distances are listed.

mentioned, the B3LYP/6-311G(d,p) method is inadequate for studies of weak interactions and the results for these exohedral noble gas complexes are therefore unreliable and will not be discussed here. All the exohedral complexes included in Table 3 are more stable than their isolated components. No exohedral argon complex was found in the present study. The F^- complex exhibits a remarkable behavior. All attempts to optimize the exohedral $F^-(HSiO_{3/2})_{10}$ yielded the endohedral $F^-@(HSiO_{3/2})_{10}$, identical with the endohedral complex formed by initially placing F^- at the center of the cage. This suggests that a fluoride ion in the vicinity of a T_{10}−POSS cage could be easily absorbed by the cage to form an endohedral complex. We did not investigate the migration path into the cage, but geometry optimizations starting from several different geometries with F^- outside the cage all yielded the same endohedral complex. This[36] suggests that the energy barrier for the entry of F^- into the cage, if any, is small. Similar behavior was also predicted for the fluoride ion and the T_8−POSS cage.[36] Among the exohedral complexes, the $Li^+(HSiO_{3/2})_{10}$ was the most stable with a binding energy of −86.2 kcal/mol.

The isomerization energies, E_{iso}, demonstrate that all the exohedral complexes $X(HSiO_{3/2})_{10}$ except the chloride and bromide complexes are more stable than the corresponding endohedral complexes. However, these isomerization energies are not sufficiently unfavorable to prevent formation of the endohedral complex. For example, $He@C_{20}H_{20}$ has been prepared despite its large unfavorable isomerization energy (35.4 kcal/mol).[56]

Electronic Properties. *Atomic Charges.* Atomic charges were calculated at the B3LYP level with the NBO method.[48] There appears to be only minor charge transfer upon complex formation. The formal +1 charge is reduced to +0.9 for the cationic endohedral complexes, and for the endohedral halide complexes the formal −1 charges are −0.8. The charges on the intercalated atom are essentially zero for the neutral noble gas and sodium and potassium complexes. However, when Li^0 is intercalated it acquires a positive charge of 0.8. No significant changes were found for the atomic charges of the POSS cages upon inclusion of any of the endohedral atoms or ions studied.

Ionization Potentials. Ionization potentials were estimated by using Koopman's theorem. Experimental (when available) and calculated ionization potentials for the endohedral complexes are summarized in Table 4. The differences between calculated and experimental values are within a reasonable range. The ionization potentials of the T_{10}−POSS encapsulated Li^0, Na^0, and K^0 are considerably lower than those of the free metal. Boldyrev and co-workers[57−59] defined species with first ionization potentials less than the Cesium atom (90.0 kcal/mol; 3.9 eV) as "superalkalis". The first ionization potential for encapsulated Li^0, Na^0, and K^0 ranges from 54.7 to 34.5 kcal/mol. These values are significantly smaller than the IP of cesium. Thus, $X@(HSiO_{3/2})_{10}$ (X = Li, Na, and K) could be considered as "superalkalis". Moran et al. observed similar behavior for the dodecahedrane endohedral complex of alkali and alkaline earth metals.[56]

TABLE 3: Total Energies (hartrees), Zero-Point Corrected Inclusion, Binding, and Isomerization Energies (kcal/mol), and Basis Set Superposition Errors (kcal/mol)

Empty T_{10}−POSS Cage	
B3LYP/6-311G**	MP2/6-311G**// B3LYP/6-311G**
−4031.427632	−4023.881090

Endohedral Complexes

	B3LYP/6-311G**			MP2/6-311G**// B3LYP/6-311G**	
X	total energy	E_{inc}	BSSE	total energy	E_{inc}
Li^+	−4038.789806	−47.1	−6.0	−4031.214928	−61.7
Li^0	−4038.893495	14.7		−4031.299076	8.7
Li^-	−4038.948852	−10.2		−4031.351404	−23.1
Na^+	−4193.553367	−23.8	−4.8	−4185.590703	−29.0
Na^0	−4193.648986	40.6		−4185.662508	42.4
Na^-	−4193.639109	53.5		−4185.637472	62.6
K^+	−4631.177345	7.0	−4.1	−4622.824110	36.8
K^0	−4631.242685	68.3		−4623.089683	69.6
K^-	−4631.220251	92.8		−4623.019895	96.6
F^-	−4131.412207	−101.5	−4.4	−4123.666052	−106.5
Cl^-	−491.760210	−19.0	−6.4	−4483.643314	−37.8
Br^-	−6650.651373	2.4	−11.5	−6596.625028	−18.0
He	−4034.335469	4.1	−0.6	−4026.761912	3.3
Ne	−4160.376129	2.3	−6.7	−4152.609736	2.7
Ar	−4558.926895	34.9	−2.9	−4550.797008	24.9

Exohedral Complexes

	B3LYP/6-311G**				MP2/6-311G**// B3LYP/6-311G**		
X	total energy	E_{bind}	BSSE	E_{iso}	total energy	E_{bind}	E_{iso}
Li^+	−4038. 815705	−64.7	4.7	−16.1	−4031.243212	−85.5	−23.7
Na^+	−4193.587173	−44.7	3.5	−20.6	−4185.617013	−43.7	−14.7
K^+	−4631.235679	−29.2	2.0	−22.2	−4622.876175	5.4	−31.4
Cl^-	−4491.750781	−14.1	2.3	4.9	−4483.607616	−15.7	22.7
Br^-	−6605.674932	−8.7	0.7	−10.0	−6596.622001	−15.8	1.6
He	−4034.372779	−20.7	0.1	−24.1	−4026.765819	0.1	−1.7
Ne	−4160.381548	−1.8	0.5	−4.1	−4152.614952	−0.5	−3.3

TABLE 4: Ionization Potentials (IP, kcal/mol) of Free Atoms and Endohedral (X@T_{10}−POSS) Complexes Calculated at the B3LYP/6-311G(d,p) Level

ionization process	IP(calcd)	IP(exptl)[a]
$Li^- \rightarrow Li + e^-$	11.6	
$Li^-@(HSi_{3/2})_{10} \rightarrow Li@(HSi_{3/2})_{10} + e^-$	34.7	
$Li \rightarrow Li^+ + e^-$	129.5	124.3
$Li@(HSi_{3/2})_{10} \rightarrow Li^+@(HSi_{3/2})_{10} + e^-$	65.1	
$Na^- \rightarrow Na + e^-$	10.3	
$Na^-@(HSi_{3/2})_{10} \rightarrow Na@(HSi_{3/2})_{10} + e^-$	2.6	
$Na \rightarrow Na^+ + e^-$	125.0	118.5
$Na@(HSi_{3/2})_{10} \rightarrow Na^+@(HSi_{3/2})_{10} + e^-$	60.6	
$K^- K + e^-$	10.1	
$K^-@(HSi_{3/2})_{10} \rightarrow K@(HSi_{3/2})_{10} + e^-$	14.1	
$K \rightarrow K^+ + e^-$	113.7	100.1
$K@(HSi_{3/2})_{10} \rightarrow K^+@(HSi_{3/2})_{10} + e^-$	41.0	

[a] References 64 and 65.

TABLE 5: Chemical Shifts[a] (ppm) for T_{10}−POSS and Selected Endohedral T_{10}−POSS Complexes Calculated at the B3LYP/6-311G(d,p) Level

system	^{29}Si	^1H	X
T_{10}−POSS cage	−93.3, −86.3[b]	4.8, 4.2[b]	
$He@(SiHO_{3/2})_{10}$	−103.0	4.7	0.8
$Li^+@(SiHO_{3/2})_{10}$	−77.2, −79.0, −84.5, −70.1, −71.6	5.3, 5.1	5.1, −2.0[c]
$F^-@(SiHO_{3/2})_{10}$	−93.1, −93.6	4.4	195.3

[a] The ^1H and ^{29}Si chemical shifts are relative to TMS. Li^+, F^-, and He chemical shifts obtained by subtracting the absolute isotropic shielding of encapsulated Li^+, F^-, and He from the corresponding unencapsulated species. [b] The experimental chemical shifts of ^1H and ^{29}Si relative to TMS. [c] The Li^+ chemical shift relative to LiCl.

NMR Chemical Shifts. Table 5 summarizes the chemical shifts for the parent $(HSiO_{3/2})_{10}$ cage and for $X@(HSiO_{3/2})_{10}$ (where guests are X = He, Li^+, and F^-) calculated at the B3LYP/6-311G(d,p) level with use of the GIAO method. [44−47] The chemical shifts for encapsulated He, Li^+, and F^- were obtained by taking the difference between the isotropic shielding of the free species and the isotropic shielding of the encapsulated analogues. Silicon and hydrogen chemical shifts are reported relative to TMS.

The He atom is slightly deshielded (0.8 ppm) by the $(HSiO_{3/2})_{10}$ cage. This is in sharp contrast with the large calculated shielding obtained by Buhl et al.[60] for $He@C_{60}H_{60}$ (−5.2 ppm) but reminiscent of the deshielding of He in $He@C_{20}H_{20}$ (1.5 ppm) predicted by Jimenez-Vazquez et al.[61] The nucleus independent chemical shift (NICS) calculated at the center of the $(HSiO_{3/2})_{10}$ cage is −0.2 ppm. For comparison the NICS value calculated at the center of the benzene ring is −11.5 and −2.1 ppm for cyclohexane.[62] No evidence exists for either aromaticity or antiaromaticity for the empty T_{10}−POSS cage based on its NICS value.

Overall, the effects of encapsulating He and F^- on the NMR spectra of $(HSiO_{3/2})_{10}$ are small. The Si^{29} chemical shifts in $He@(HSiO_{3/2})_{10}$, $Li^+@(HSiO_{3/2})_{10}$, and $F^-@(HSiO_{3/2})_{10}$ chemical shifts are shifted relative to those of $(HSiO_{3/2})_{10}$ by 9.7 ppm, −7.3 to −23.2 ppm, respectively. The ^1H chemical shifts in $Li^+@(HSiO_{3/2})_{10}$ and $F^-@(HSiO_{3/2})_{10}$ are displaced by 0.4 ppm and −0.2 to −0.3 ppm, respectively, relative to $(HSiO_{3/2})_{10}$.

TABLE 6: Total Energies (hartrees), Binding Energies (kcal/mol), Li−F Bond Lengths (Å), and Natural Charges for the LiF Complex with T_{10}−POSS

system[a]	sym	total energy B3LYP[b]	E_{bind} B3LYP[b]	r_{Li-F}	natural charges	total energy MP2[c]	E_{bind} MP2[c]
F^-@Li^+ T_{10}−POSS (D5R)	C_s	−4138.945508	−255.4	1.741	Li 0.2, F −0.6	−4131.186091	−282.4
F^-@Li^+ T_{10}−POSS (D4R)	C_{2v}	−4138.895918	−229.6	2.738	Li 0.2, F −0.6	−4131.172645	−274.5

[a] See text. [b] B3LYP/6-311G**//B3LYP/6-311G**. [c] MP2/6-311G**//B3LYP/6-311G**.

Therefore, ^{1}H NMR will be a useful tool to detect and identify Li^+@$(HSiO_{3/2})_{10}$ and F^-@$(HSiO_{3/2})_{10}$ while ^{29}Si NMR can be used to characterize He@$(HSiO_{3/2})_{10}$ and Li^+@$(HSiO_{3/2})_{10}$.

Presence of Counterion. An electrically charged chemical complex would coexist with a counterion. The effect of a counterion was investigated by using LiF as an example. Initially, geometry optimizations were performed from two different starting geometries, one by placing both Li^+ and F^- ions 1 Å apart inside the cage, and one with the F^- ion at the center of the cage and a Li^+ outside the D5R surface, 3.4 Å from the center of the cage. The second geometry is reminiscent of the ammonium F^-@T_8−POSS salt synthesized and characterized by Taylor.[63] Table 6 summarizes energies, zero-point corrected binding energies, bond lengths, and charge on the encapsulated Li^+ and F^-. Both starting geometries converged to the same optimized structure. The F^- ion remained inside the cage with the Li^+ ions situated on one of the cage's D5R surfaces. The fluoride ion has moved off center toward the lithium ion. The Li−F distance in the complex is 1.741 Å. For comparison, the experimental LiF distance in gaseous LiF is 1.55 Å and the LiF bond length calculated at the B3LYP/6-311G(d,p) level is also 1.55 Å. The LiF bond of this complex is thus somewhat weaker than in gaseous LiF and the calculated atomic charges also indicate a reduction in the dipolar nature of LiF in the complex.

The calculated inclusion energy for this complex is −282.4 kcal/mol. The inclusion energy relative to F^- and $Li^+(HSiO_{3/2})_{10}$ is −206.8 kcal/mol while the binding energy relative to Li^+ and F^-@$(HSiO_{3/2})_{10}$ is −178.3 kcal/mol. For comparison the endohedral inclusion energy for the fluoride ion and the binding energy for the lithium ion were −106.5 and −86.2.0 kcal/mol, respectively, suggesting that the counterion stabilizes the complexes significantly. A large part of this stabilization originates from the formation of a relatively strong LiF bond. However, the energy of the complex is still 60.8 kcal/mol lower than the sum of the energy of LiF and the empty POSS−T_{10} cage in spite of the stretched LiF bond in the complex.

We also investigated a structure with the F^- ion placed inside and the Li^+ ion initially placed outside of the D4R surface of the T_{10}−POSS cage 3.4 Å from the center of the cage. The resulting structure, referred to as the D4R complex (Table 6), lies about 8 kcal/mol above the other (D5R) LiF T_{10}−POSS complex and the LiF distance in the D4R complex (2.738 Å) is much longer (see Table 6) than that in the D5R complex.

IV. Conclusions

The following conclusions can be drawn from these theoretical calculations. The formation of the endohedral complexes Li^+@$(HSiO_{3/2})_{10}$, Na^+@$(HSiO_{3/2})_{10}$, F^-@$(HSiO_{3/2})_{10}$, Cl^-@$(HSiO_{3/2})_{10}$, and Br^-@$(HSiO_{3/2})_{10}$ from their isolated components is energetically favorable in each case. These ions are thermodynamically stable within the $(HSiO_{3/2})_{10}$ cage. All exohedral X$(HSiO_{3/2})_{10}$ except the chloride and bromide complexes have lower energies than their endohedral counterparts. No exohedral F^- complex exists, as all exohedral starting geometries resulted in the endohedral complex.

Endohedral complexes with the neutral alkali metals have far smaller first ionization potentials (IP) than that of atomic cesium and are thus " superalkalis ". Calculated NMR chemical shifts of endohedral He (0.8 ppm), Li^+ (5.1 ppm), and F^- (195.3 ppm) nuclei indicate considerable deshielding compared to the corresponding isolated species. The NICS value computed at the center of the $(HSiO_{3/2})_{10}$ cage shows no evidence for any aromaticity or antiaromaticity in the cage molecule.

Acknowledgment. This work was supported by a grant from Air Force Office of Scientific Research Grant No. F49620-02-1-026-0, by the National Science Foundation Grant Nos. EPS 0132618, HRD-9805465, and DMR-0304036, by the National Institutes of Health through the Grant No. S06-GM008047, by the Army High Performance Computing Research Center under the auspices of Department of the Army, Army Research Laboratory under Cooperative Agreement No. DAAD 19-01-2-0014, and by the Department of Defense through the US Army/Engineer Research and Development Center (Vicksburg, MS), Contract #W912HZ-06-C-0057.

References and Notes

(1) Fu, B. X.; Hsiao, B. S.; Pagola, S.; Stephens, P.; White, H.; Rafailovich, M.; Sokolov, J.; Mather, P. T.; Jeon, H. G.; Philips, S.; Lichtenhan, J.; Schwab, J. *Polymer* **2001**, *42*, 599.
(2) Maitra, P.; Wunder, S. L. *Electrochem. Solid-State Lett.* **2004**, *7*, A88.
(3) Romo-Uribe, A.; Mather, P. T.; Haddad, T. S.; Lichtenhan, J. D. *J. Polym. Sci., Part B*: *Polym. Phys.* **1998**, *36*, 18571872.
(4) Li, G.; Wang, L.; Ni, H.; Pittman, C. U., Jr. *J. Inorg. Organomet. Polym.* **2002**, *11*, 123.
(5) Agaskar, P. A.; Klemperer, W. G. *Inorg. Chim. Acta* **1995**, *229*, 355.
(6) Brown, J. F., Jr.; Vogt, L. H., Jr. *J. Am. Chem. Soc.* **1965**, *87*, 4313.
(7) Feher, F. J.; Wyndham, K. D. *Chem. Commun.* **1998**, 323.
(8) Li, G. Z.; Wang, L.; Toghiani, H.; Daulton, T. L.; Koyama, K.; Pittman, C. U., Jr. *Macromolecules* **2001**, *34*, 8686.
(9) Li, G. Z.; Wang, L.; Toghiani, H.; Daulton, T. L.; Pittman, C. U. *Polymer* **2002**, *43*, 4167.
(10) Maxim, N.; Magusin, P. C. M. M.; Kooyman, P. J.; van Wolput, J. H. M. C.; van Santen, R. A.; Abbenhuis, H. C. L. *Chem. Mater.* **2001**, *13*, 2958.
(11) Maxim, N.; Overweg, A.; Kooyman, P. J.; van Wolput, J. H. M. C.; Hanssen, R. W. J. M.; van Santen, R. A.; Abbenhuis, H. C. L. *J. Phys. Chem. B* **2002**, *106*, 2203.
(12) Zheng, L.; Waddon, A. J.; Farris, R. J.; Coughlin, E. B. *Macromolecules* **2002**, *35*, 2375.
(13) Wada, K.; Yamada, K.; Kondo, T.; Mitsudo, T.-A. *Chem. Lett.* **2001**, 12.
(14) Dance, B. *Semiconduct. Int.* **2001**, *24*, 46.
(15) Lamm, M. H.; Chen, T.; Glotzer, S. C. *Nano Lett.* **2003**, *3*, 989.
(16) Fu, B. X.; Hsiao, B. S.; White, H.; Rafailovich, M.; Mather, P. T.; Jeon, H. G.; Phillips, S.; Lichtenhan, J.; Schwab, J. *Polym. Int.* **2000**, *49*, 437.
(17) Lee, A.; Lichtenhan, J. D. *J. Appl. Polym. Sci.* **1999**, *73*, 1993.
(18) Haddad, T. S.; Lichtenhan, J. D. *Macromolecules* **1996**, *29*, 7302.
(19) Schwab, J. J.; Lichtenhan, J. D. *Appl. Organomet. Chem.* **1998**, *12*, 707.
(20) Raj, R.; Riedel, R.; Soraru, G. D. *J. Am. Ceram. Soc.* **2001**, *84*, 2158.
(21) Abbenhuis, H. C. L. *Chem. Eur. J.* **2000**, *6*, 25.
(22) Ducateau, R.; Cremer, U.; Harmsen, R. J.; Mohamud, S. I.; Abbenhuis, C. L.; Avan Saten, R.; Meetsma, A.; Thiele, S. K.-H.; van Tol, F. F. H.; Kranenburg, M. *Organometallics* **1999**, *18*, 5447.
(23) Klunduk, M. C.; Maschmeyer, T.; Thomas, J. M.; Johnson, F. G. *Chem. Eur. J.* **1999**, *5*, 1481.

(24) Pescarmona, P. P.; Van der Waal, J. C.; Maxwell, I. E.; Maschmeyer, T. *Angew. Chem., Int. Ed.* **2001**, *40*, 740.
(25) Xiao, F. S.; Han, Y.; Yu, Y.; Meng, X.; Yang, M.; Wu, S. *J. Am. Chem. Soc.* **2002**, *124*, 888.
(26) Liu, J. C. *Appl. Organomet. Chem.* **1999**, *13*, 295.
(27) de Vos, R. M.; Verweij, H. *J. Membr. Sci.* **1998**, *143*, 37.
(28) Suzuki, F.; Nakane, K.; Yasuo, H. *J. Membr. Sci.* **1995**, *104*, 183.
(29) McCusker, C.; Carroll, J. B.; Rotello, V. M. *Chem. Commun.* (*Cambridge, U.K.*) **2005**, 996.
(30) Zahang, C.; Babonneau, F.; Bonhomme, C.; Laine, R. M.; Soles, C. L.; Hristov, A. H.; Yee, F. A. *J. Am. Chem. Soc.* **1998**, *120*, 8380.
(31) Cheng, W.-D.; Xiang, K.-H.; Pandey, R.; Pernisz, U. C. *J. Phys. Chem. B* **2000**, *104*, 6737.
(32) Päch, M.; Stösser, R. *J. Phys. Chem. A* **1997**, *101*, 8360.
(33) George, A. R.; Catlow, C. R. A. *Chem. Phys. Lett.* **1995**, *247*, 408.
(34) Bassindale, A. R.; Pourny, M.; Taylor, P. G.; Hursthouse, M. B.; Light, M. E. *Angew. Chem., Int. Ed.* **2003**, *42*, 3488.
(35) Tejerina, B.; Gordon, M. S. *J. Phys. Chem. B* **2002**, *106*, 11764.
(36) Park, S. S.; Xiao, C.; Hagelberg, F.; Hossain, D.; Pittman, C. U., Jr.; Saebo, S. *J. Phys. Chem. A* **2004**, *108*, 11260.
(37) Allen, E. C.; Beers, K. J. *Polymer* **2005**, *46*, 569.
(38) Earley, C. W. *J. Phys. Chem.* **1994**, *98*, 8693.
(39) Lee, C.; Yang, W.; Parr, R. G. *Phys. Rev. B*: *Condens. Matter Mater. Phys.* **1988**, *37*, 785.
(40) Becke, A. D. *J. Chem. Phys.* **1993**, *98*, 5648.
(41) Frisch, M. J.; Pople, J. A.; Binkley, J. S. *J. Chem. Phys.* **1984**, *80*, 3265.
(42) Frisch, M. J.; Trucks, G. W.; Schlegel, H. B.; Scuseria, G. E.; Robb, M. A.; Cheeseman, J. R.; Montgomery, J. A., Jr.; Vreven, T.; Kudin, K. N.; Burant, J. C.; Millam, J. M.; Iyengar, S. S.; Tomasi, J.; Barone, V.; Mennucci, B.; Cossi, M.; Scalmani, G.; Rega, N.; Petersson, G. A.; Nakatsuji, H.; Hada, M.; Ehara, M.; Toyota, K.; Fukuda, R.; Hasegawa, J.; Ishida, M.; Nakajima, T.; Honda, Y.; Kitao, O.; Nakai, H.; Klene, M.; Li, X.; Knox, J. E.; Hratchian, H. P.; Cross, J. B.; Bakken, V.; Adamo, C.; Jaramillo, J.; Gomperts, R.; Stratmann, R. E.; Yazyev, O.; Austin, A. J.; Cammi, R.; Pomelli, C.; Ochterski, J. W.; Ayala, P. Y.; Morokuma, K.; Voth, G. A.; Salvador, P.; Dannenberg, J. J.; Zakrzewski, V. G.; Dapprich, S.; Daniels, A. D.; Strain, M. C.; Farkas, O.; Malick, D. K.; Rabuck, A. D.; Raghavachari, K.; Foresman, J. B.; Ortiz, J. V.; Cui, Q.; Baboul, A. G.; Clifford, S.; Cioslowski, J.; Stefanov, B. B.; Liu, G.; Liashenko, A.; Piskorz, P.; Komaromi, I.; Martin, R. L.; Fox, D. J.; Keith, T.; Al-Laham, M. A.; Peng, C. Y.; Nanayakkara, A.; Challacombe, M.; Gill, P. M. W.; Johnson, B.; Chen, W.; Wong, M. W.; Gonzalez, C.; Pople, J. A. *Gaussian-03*; Gaussian, Inc.: Wallingford, CT, 2004.
(43) *PQS* version 3.1, Parallel Quantum Solutions: 2013 Green Acres Road, Fayetteville, AR 72703. *PQS* version 3.1; Parallel Quantum Solutions: 2013 Green Acres Road, Fayetteville, AR 72703.
(44) Wolinski, K.; Hinton, J. F.; Pulay, P. *J. Am. Chem. Soc.* **1990**, *112*, 8251.
(45) Schreckkenbach, G.; Ziegler, T. *J. Phys. Chem.* **1995**, *99*, 606.
(46) Cheeseman, J. R.; Trucks, G. W.; Keith, T.; Frisch, M. J. *J. Phys. Chem.* **1996**, *104*, 5497.
(47) Ditchfield, R. *J. Chem. Phys.* **1976**, *65*, 3123.
(48) Glendening, E. D.; Reed, A. E.; Carpenter, J. E.; Weinhold, F. *NBO 4.M*; University of Wisconsin: Madison, WI, 1993.
(49) Boys, S. F.; Bernardi, F. *Mol. Phys.* **1970**, *19*, 553.
(50) Heyde, T. P. E.; Burgi, H.-B.; Burgi, H.; Tornroos, K. W. *Chimia* **1991**, *45*, 38.
(51) de Man, A. J. M.; Sauer, J. *J. Phys. Chem.* **1996**, *100*, 5025.
(52) Tossell, J. A. *J. Phys. Chem.* **1996**, *100*, 5025.
(53) Xiang, K.-H.; Pandey, R.; Pernisz, U. C.; Freeman, J. *J. Phys. Chem. B* **1998**, *102*, 8704.
(54) Pasquarello, A.; Hybertsen, M. S.; Car, R. *Phys. Rev. B* **1996**, *54*, R2339.
(55) Sun, Q.; Wang, Q.; Yu, J. Z.; Ohno, K.; Kawazoe, Y. *J. Phys.: Condens. Matter* **2001**, *13*, 1931.
(56) Moran, D.; Stahl, F.; Jemmis, E. D.; Schaefer, H. F., III; Schleyer, P. v. R. *J. Phys. Chem. A* **2002**, *106*, 5144.
(57) Rehm, E.; Boldyrev, A. I.; Schleyer, P. v. R. *Inorg. Chem.* **1992**, *31*, 4831.
(58) Gutsev, G. L.; Boldyrev, A. I. *Chem. Phys. Lett.* **1982**, *92*, 262.
(59) Gutsev, G. L.; Boldyrev, A. I. *Adv. Chem. Phys.* **1985**, *61*, 169.
(60) Buhl, M.; Thiel, W.; Jiao, H.; Schleyer, P. v. R.; Saunders, M.; Anet, F. A. L. *J. Am. Chem. Soc.* **1994**, *116*, 6005.
(61) Jimenez-Vazquez, H. A.; Tamariz, J.; Cross, R. J. *J. Phys. Chem. A* **2001**, *105*, 1315.
(62) Jiao, H.; Nagelkerke, R.; Kurtz, H. A.; Williams, R. V.; Borden, W. T.; Schleyer, P. v. R. *J. Am. Chem. Soc.* **1997**, *119*, 5921.
(63) Bassindale, A. R.; Baukov, Y. I.; Borbaruah, M.; Glynn, S. J.; Negrebetsky, V. V.; Parker, D. J.; Taylor, P. G.; Turtle, R. *J. Org. Chem.* **2003**, *669*, 154.
(64) Huheey, E. J.; Keiter, A. E.; Keiter, L. R. *Inorganic Chemistry*: *Principles of Structure and Reactivity*; HarperCollins: New York, 1993.
(65) James, M. A.; Lord, P. M. *Macmillan's Chemical and Physical Data*; Macmillan: London, UK, 1992.